Journal of Alloys and Compounds 509 (2011) 3866–3871

Contents lists available at ScienceDirect

Journal of Alloys and Compounds

journal homepage: www.elsevier.com/locate/jallcom

Hydrothermal synthesis of YBO_3:Tb^{3+} microflowers and their luminescence properties

Lan Yang, Liqun Zhou*, Xiange Chen, Xiaolan Liu, Pei Hua, Yan Shi, Xiaoguang Yue, Ziwei Tang, Ying Huang

Ministry of Education, Key Laboratory for the Synthesis and Application of Organic Functional Molecules and College of Chemistry and Chemical Engineering, Hubei University, Wuhan 430062, PR China

ARTICLE INFO

Article history:
Received 23 June 2010
Received in revised form
16 December 2010
Accepted 17 December 2010
Available online 24 December 2010

Keywords:
YBO_3
Tb^{3+}
Microstructure
Crystal growth
Luminescence

ABSTRACT

Three-dimensional flowerlike YBO_3:Tb^{3+} phosphors have been successfully prepared by an efficient surfactant-free hydrothermal process directly without further sintering treatment. X-ray diffraction (XRD), scanning electron microscopy (SEM), transmission electron microscopy (TEM), energy-dispersive X-ray (EDS) spectrometry, selected area electron diffraction (SAED), photoluminescence (PL) spectra were used to characterize the samples. The as-obtained samples present flowerlike agglomerates composed of nanoflakes with thickness of 20 nm and high crystallinity in spite of the moderate reaction temperature of 180 °C. The reaction mechanism has been considered as a dissolution/precipitation mechanism; the self-assembly evolution process has been proposed on homocentric layer-by-layer growth style. The different luminescent intensity with different molar ratio of Y–Tb [Y:Tb = 8:2; 7:3; 6:4; 5:5; 4:6], YBO_3:Tb^{3+} phosphors exhibit different light (white, red, green) under ultraviolet excitation, which might find potential applications in the fields such as light display systems and optoelectronic devices.

1. Introduction

Recently, orthoborate phosphors are widely used in field-emission displays (FEDs), plasma display panels (PDPs), cathode ray tubes (CRTs) and a new generation of Hg-free fluorescent lamps [1,2]. Among the orthoborate phosphors, YBO_3-based phosphors have attracted much attention due to their low toxicity, strong luminescence intensity, high chemical stability, and exceptional optical damage threshold [3–5]. YBO_3:Tb^{3+} phosphor is regarded as one of the potential green phosphors to be utilized in PDPs [6]. It has a strong absorption band in the vacuum ultraviolet (VUV) range, and its luminance under VUV excitation is as high as conventional commercial green phosphors. Therefore, research on preparation and luminescence property of YBO_3:Tb^{3+} phosphor is of great importance.

YBO_3:Tb^{3+} phosphor has been synthesized via various routes, such as solid-state reaction [7], sol–gel method [1,8], spray pyrolysis method [9] and hydrothermal method [10]. Compared to the other routes, the hydrothermal method is a promising synthetic route, which can be better controlled from the molecular precursor to the reaction parameters, such as the reaction time and temperature, to give highly pure and homogeneous materials. The technique allows low reaction temperatures, and controllable size and morphology of the products [11]. Although there have been some reports about the hydrothermal synthesis and properties of rare earth orthoborate YBO_3:Tb^{3+}, all of them were focused on YBO_3:Tb^{3+} which show the characteristic green emission under VUV excitation. To the best of our knowledge, few studies about hydrothermal synthesis of YBO_3:Tb^{3+} which show strong red/white light emission under VUV excitation have been reported.

Herein we report an efficient surfactant-free hydrothermal approach to synthesize hexagonal YBO_3:Tb^{3+} with novel self-assembled 3D architectures. These microflowers, which were composed of nanosized units, were expected to maintain the desirable properties of YBO_3:Tb^{3+} nanocrystals (flakes) while being quite stable on the micrometer scale. In spite of the moderate reaction temperature of 180 °C, the as-synthesized YBO_3:Tb^{3+} is highly crystalline. The luminescent properties of the flowerlike YBO_3:Tb^{3+} composed of nanoflakes have also been investigated.

2. Experimental

All chemicals were analytically pure and were used without further purification. For the synthesis of the YBO_3:Tb^{3+} microflowers, 10 mL of an aqueous solution (0.2 mol L^{-1}) of yttrium nitrate hexahydrate [$Y(NO_3)_3{\cdot}6H_2O$] mixed with Tb^{3+}, according to the molar ratio Y:Tb = 8:2, 7:3, 6:4, 5:5, 4:6, respectively, was prepared. Then, 0.3708 g (6 mmol) of H_3BO_3 (100% excess) were mixed under stirring and deionized water was added to the above mixture to reach 40 mL for total volume. The solution was stirred for another 30 min to form a clear aqueous solution. Then 25 wt% of $NH_3{\cdot}H_2O$ (A.R.) was introduced dropwise to the vigorously stirred

* Corresponding author. Tel.: +86 27 50865540; fax: +86 27 88663043.
E-mail addresses: zlq@hubu.edu.cn, yanglan1116@126.com (L. Zhou).

0925-8388/$ – see front matter © 2011 Elsevier B.V. All rights reserved.
doi:10.1016/j.jallcom.2010.12.128

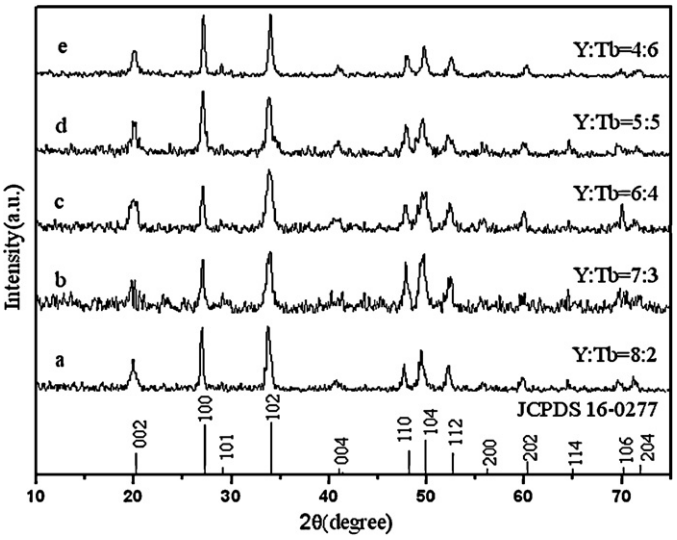

Fig. 1. XRD patterns for the YBO_3:Tb^{3+} samples with the different molar ratio of Y–Tb [Y:Tb = 8:2 (a); 7:3 (b); 6:4 (c); 5:5 (d); 4:6 (e)] obtained from the hydrothermal process.

solution until pH = 7. After additional agitation for 40 min, the as-obtained white colloidal precipitate was transferred to a 50 mL autoclave, sealed, and heated at 180 °C for 3 days. It was then cooled to room temperature naturally. The products were then collected by filtration, washed with ethanol and deionized water for several times, and dried in atmosphere at 80 °C for 24 h.

The phase purity and crystallinity of all the samples were examined by powder X-ray diffraction (XRD) performed on a Rigaku D/max-3C X-ray diffractometer with Cu Kα radiation (1.54 Å), the operation voltage and current were 40 kV and 40 mA, respectively. The morphology and structure of the samples were inspected using field emission scanning electron microscope (FE-SEM, Philips XL30 TMP) and field emission transmission electron microscopy (TEM, FEI Tecnai G20) equipped with energy-dispersive X-ray (EDS) spectrometer and selective area electron diffraction (SAED). Photoluminescence (PL) excitation and emission spectra were taken on a Jasco FP-6500 spectrofluorometer equipped with a 150 W xenon lamp as the excitation source at room temperature.

3. Results and discussion

3.1. Crystallite structure, morphology analyses

It is well known that rare earth ions have similar radius, coordination structure and physical-chemical properties. When one Y^{3+} is replaced by Tb^{3+}, the crystal structure does not change dramatically [12]. The crystalline structure and phase purity of all the as-formed YBO_3:Tb^{3+} flowerlike products through the hydrothermal process were characterized by X-ray diffraction (XRD) and showed similar crystalline structure. All diffraction peaks of the as-obtained white products (Fig. 1) can be readily indexed to the pure hexagonal phase of YBO_3 crystal [space group: $P63/m$ (176)] with a vaterite structure according to the JCPDS file No. 16-0277. No additional peaks of other phases have been found, indicating that Tb^{3+} has been effectively built into the host lattice. Take YBO_3:Tb^{3+} (Y:Tb = 8:2, in molar ratio) as representative (Fig. 1a). The calculated lattice constants, $a = b = 0.3793$ nm, $c = 0.8832$ nm is well compatible with the literature values of $a = b = 0.3778$ nm, $c = 0.8871$ nm (YBO_3, JCPDS 16-0277). Therefore, it can be concluded that phase-pure YBO_3:Tb^{3+} products can be obtained by the hydrothermal method.

Although all peaks of the as-formed YBO_3:Tb^{3+} flowerlike products through the hydrothermal process can be assigned to the standard data of YBO_3 (JCPDS No. 16-0277), small XRD peaks at around 47.92°, 49.63°, 57.47°, 69.86°, 71.72° which can be indexed as the (1 1 0), (1 0 4), (1 1 2), (1 0 6) and (2 0 4) peaks shift from the values of the standard card. It can be due to the difference in ionic radius between Y^{3+} and Tb^{3+}. In conclusion, the as-formed YBO_3:Tb^{3+} flowerlike products are phase-pure YBO_3:Tb^{3+} products with high crystallinity.

The SEM images of the YBO_3:Tb^{3+} (Y:Tb = 5:5, in molar ratio) sample are shown in Fig. 2a–c, which show that the sample consists of microflowers nearly monodispersed and their diameters are around from 5 to 15 μm. Detailed surface observation is presented in Fig. 2b and c which reveals that the microflower is constructed by densely packed nanoflakes with a thickness of about 20 nm. The microflowers are loosely packed and highly, and most of nanoflakes are linked together by both edge-to-edge and edge-to-surface conjunctions; the nanoflakes extend outward from the center of the microstructure, and a few of them attach to each other. Therefore, such an architecture is a result of some type of self-assembly [13,14]. The EDS spectrum (Fig. 2d) was employed to determine the chemical composition of the as-obtained products. The result reveals the presence of Y, O, B and Tb. The corresponding atomic ratio of is about 1:3:1:1, which suggests that the product may be YBO_3:Tb^{3+}, agreeing with the XRD analysis above.

The structure and morphology of the same sample was further investigated by transmission electron microscopy (TEM), as shown in Fig. 3. Clearly, a single nanofake (Fig. 3a) is assembled from nanoparticles and other nanoflakes extend outward from the center of the microstructure (Fig. 3b). During continuous growth, the extended parts of the nanoflakes are linked together by both edge-to-edge and edge-to-surface conjunctions and finally form a crystal with a flower-like structure (Fig. 3c). The hexagonal symmetry and structure of crystals are critical to direct the intrinsic shapes of the produced particles [15]. While the crystal growth is progressing, a spontaneous self-assembly process occurs in the initial step by the van der Waals attraction [16], therefore, adjacent nanocrystals or anisotropic subunits aggregate following the flower-like structure growth model [17]. The corresponding selected-area electron diffraction (SAED) pattern of the nanoflake structure (Fig. 3d) indicates the nanoflake is characteristic of a hexagonal YBO_3:Tb^{3+}, in good accordance with the XRD result. Moreover, SAED patterns taken from both different areas on a single nanoflake and different nanoflakes were found to be identical within experimental accuracy, indicating that the YBO_3:Tb^{3+} nanoflakes are single-crystalline and that different nanoflakes have identical crystallization habits. The patterns also reveal that the nanoflakes are stable enough to withstand the irradiation of convergent high-energy electron beams.

3.2. Possible formation mechanism of YBO_3:Tb^{3+} microflowers

Although the exact mechanism for the formation of these flowers is still unclear, it is believed that the growth of the flowerlike morphology is not assisted by a catalyst or directed by a template. It is well known that the chemical growth of materials inevitably involves the process of a solid phase from solution which basically consists of a nucleation step followed by particle growth stages [18]. The growth mechanism of the microflowers YBO_3:Tb^{3+} crystals could be proposed as follows. Firstly, the dissolution of the amorphous precipitates should occur, which precipitated to become the nuclei and quickly grew into nanoflakes due to the natural growing habit of forming a flakelike morphology (2D structure) with a highly anisotropic structure during the growth process of rare earth orthoborates [19–21]. Consequently, other tiny nanoflakes extend at an angle to the plane of the first flake from the center to form primary microflowers at the expense of the amorphous precipitates and/or small crystals. The primary microflowers continued to grow in a homocentric layer-by-layer growth style [22] and hierarchical flowerlike structures are formed to reduce the surface energy.

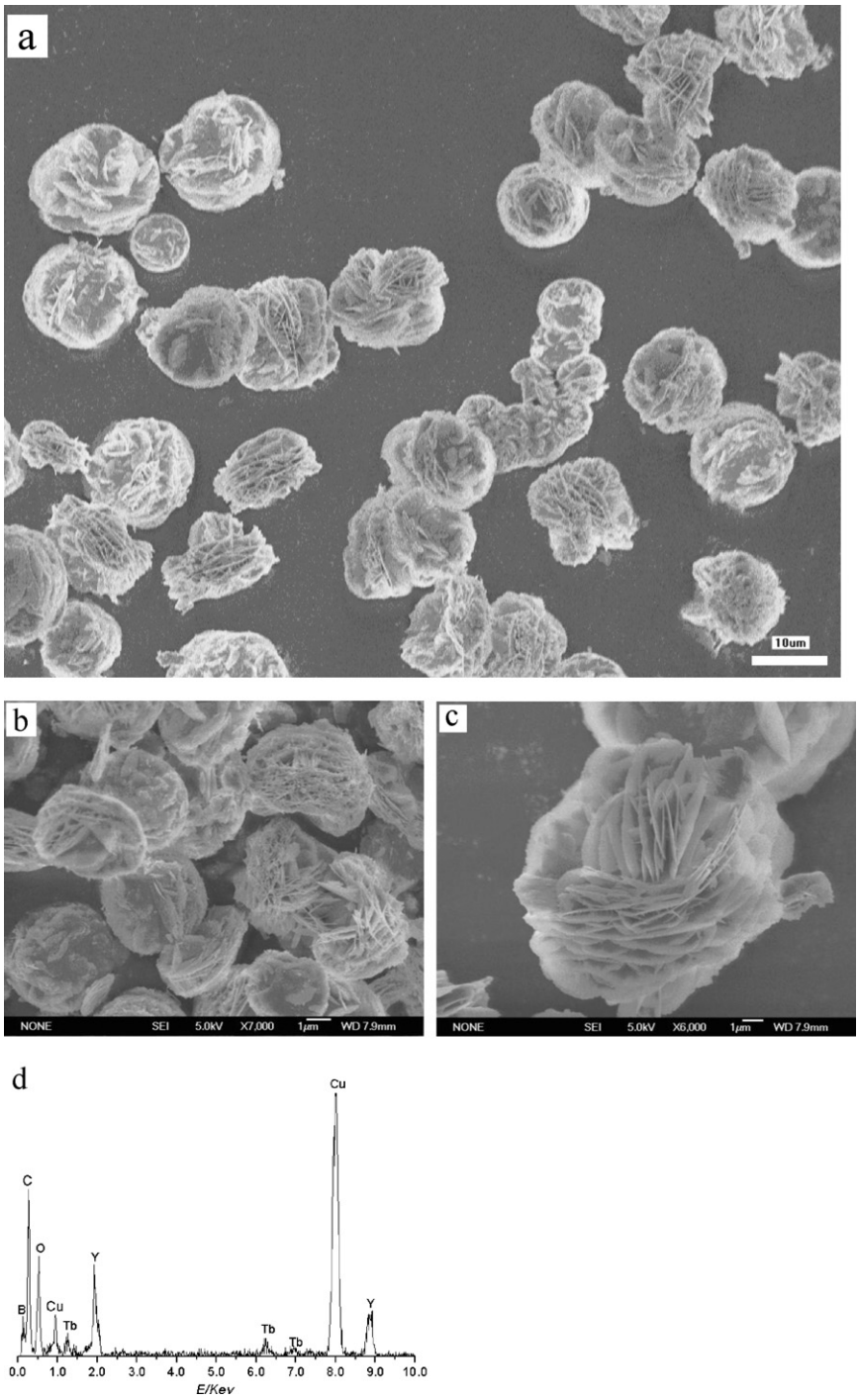

Fig. 2. SEM images of the YBO_3:Tb^{3+} (Y/Tb = 5:5) sample (a–c), EDS analysis of the as-prepared YBO_3:Tb^{3+} (Y:Tb = 5:5) (d).

On the basis of the foregoing analysis, a possible schematic illustration (Fig. 4) of the major steps involved a fast nucleation of amorphous primary particles followed by a slow aggregation and crystallization of primary particles [23]. The mechanism for the formation of the final structure morphology by interaction between primary particles remains a mystery to materials chemists [24], although many kinds of flowerlike 3D structures have been reported [11,15,24]. Several factors, including crystal-face attraction, electrostatic and dipolar fields associated with the aggregate, van der Waals forces, hydrophobic interactions and hydrogen bonds, may have various effects on the self-assembly [25].

3.3. Luminescence properties of YBO_3:Tb^{3+}

The luminescence properties of the flowerlike YBO_3:Tb^{3+} composed of nanoflakes have also been studied. Typical luminescence excitation spectra of YBO_3:Tb^{3+} phosphors are shown in Fig. 5. The excitation spectra show the similar features; we selected YBO_3:Tb^{3+} (Y:Tb = 5:5) as representative and the excitation spectrum monitored with 545 nm emission of Tb^{3+} consists of two bands with maximum at 238 and 281 nm in the range of 200–300 nm in the UV excitation spectrum due to the f–d transitions of Tb^{3+} in the YBO_3 lattice. The ground state ($4f^8$) of the Tb^{3+} belongs to ^7F_J configuration; when one electron is promoted

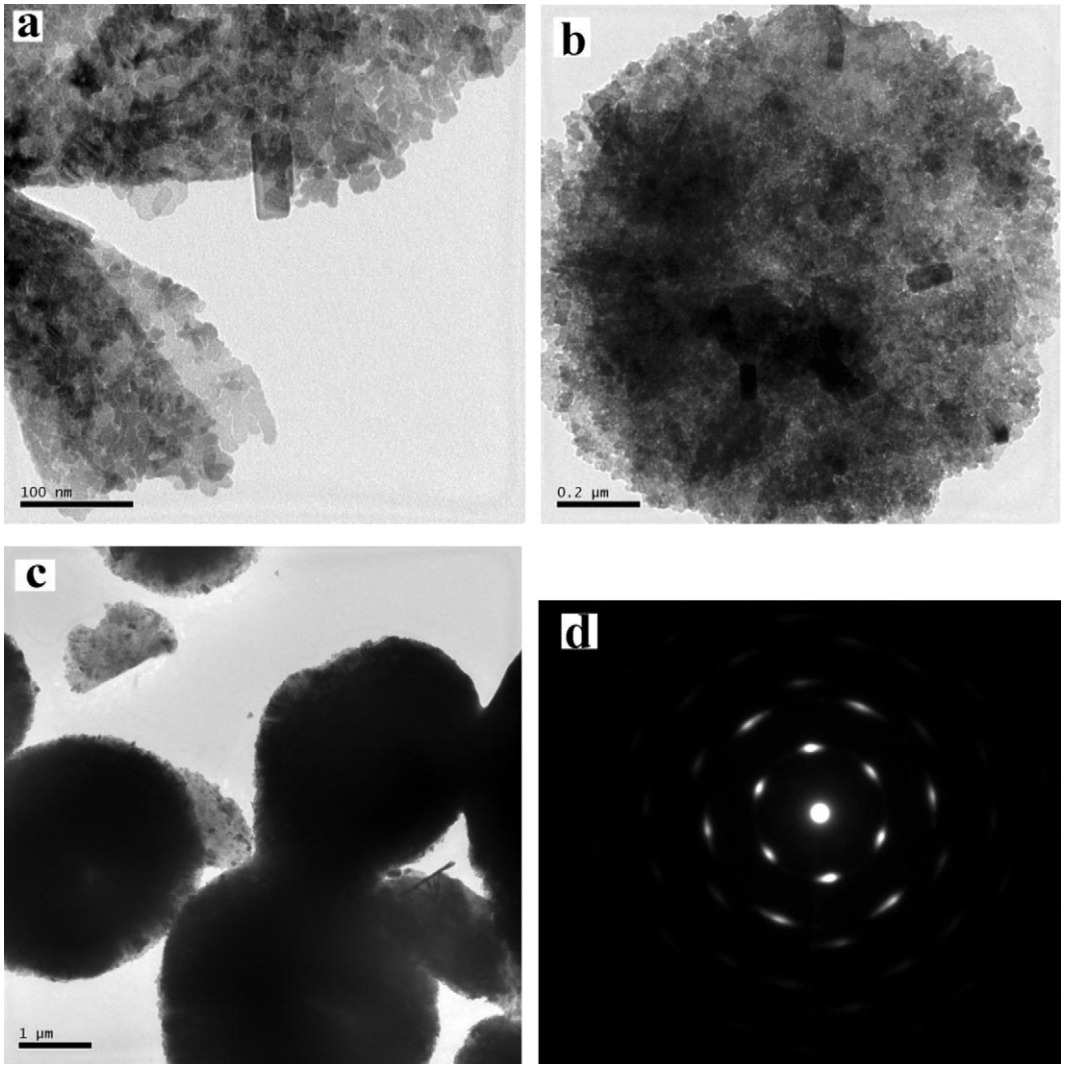

Fig. 3. TEM images of the YBO_3:Tb^{3+}(Y:Tb = 5:5) sample (a–c), SAED spectrum of YBO_3:Tb^{3+}(Y:Tb = 5:5) (d).

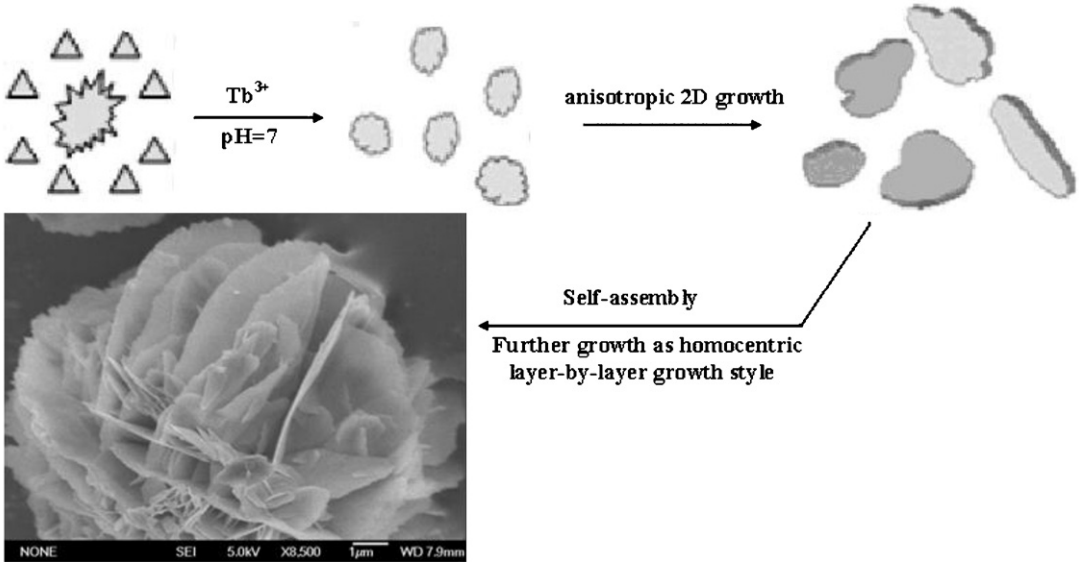

Fig. 4. Schematic illustration of the formation of the YBO_3:Tb^{3+} flowerlike structure.

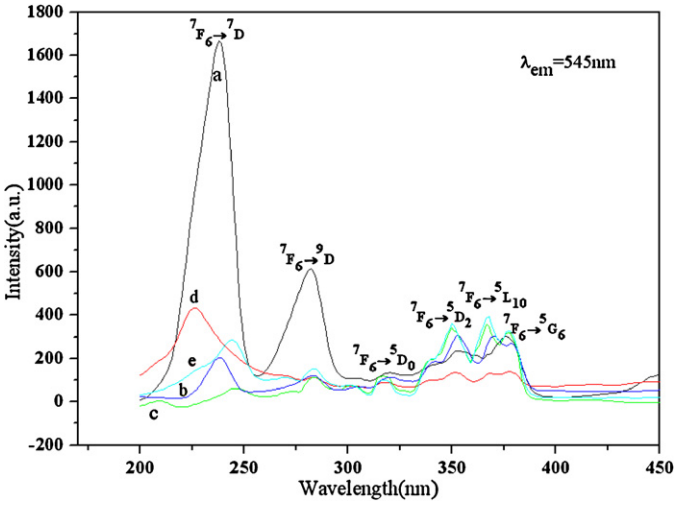

Fig. 5. Excitation spectrum of YBO_3:Tb^{3+} samples with the different molar ratio of Y–Tb [Y:Tb = 8:2 (a); 7:3 (b); 6:4 (c); 5:5 (d); 4:6 (e)].

to the 5d shell, it gives rise to two excited states belonging to $4f^7 5d^1$ configuration: the high-spin ^9D_J state and the ^7D_J low-spin state. Obviously, ^9D_J states will be lower in energy according to Hund's rule, and the transitions between ^7F_J and ^7D_J are spin-allowed, while the transitions between ^7F_J and ^9D_J are spin-forbidden. Therefore, Tb^{3+} in a specific host exhibits two groups of f–d transitions: the spin-allowed $4f^8 \rightarrow 4f^7 5d^1$ ($^7F_6 \rightarrow {}^7D$) transition with higher energy (238 nm) and the spinforbidden $4f^8 \rightarrow 4f^7 5d^1$ ($^7F_6 \rightarrow {}^9D$) transition with lower energy (281 nm) of the Tb^{3+} ion, respectively [11,26]. In the longer wavelength region, the lines corresponding to f-f transitions of Tb^{3+} which are weaker compared to f–d transitions of Tb^{3+} (Fig. 5) can be observed. These are assigned to the transitions from the $^7F_6$ ground state to the different excited states of Tb^{3+}, as 301 nm ($^5H_6$), 318 nm ($^5D_0$), 352 nm ($^5D_2$), 366 nm ($^5L_{10}$), 376 nm ($^5G_6$), respectively [11].

Fig. 6a–e shows the corresponding emission spectra of YBO_3:Tb^{3+} monitored at 281 nm, which have been measured in the range of 450–740 nm. The emission spectra consist of the f–f transition lines within $4f^8$ electron configuration of Tb^{3+}, i.e., $^5D_4 \rightarrow {}^7F_6$ (489 nm) in the blue region and $^5D_4 \rightarrow {}^7F_5$ (545 nm) in the green region, as well as $^5D_4 \rightarrow {}^7F_4$ (593 nm), $^5D_4 \rightarrow {}^7F_3$ (613 nm, 627 nm), $^5D_4 \rightarrow {}^7F_2$ (652 nm), $^5D_4 \rightarrow {}^7F_1$ (676 nm), $^5D_4 \rightarrow {}^7F_0$ (709 nm) in the red region [27]. Fig. 6f shows the emission spectrum of the commercial phosphor $CeMgAl_{11}O_{19}$:Tb.The luminescent intensity of the green emission $^5D_4 \rightarrow {}^7F_5$ (545 nm) of $CeMgAl_{11}O_{19}$:Tb is about 225 a.u. By compared with the as-obtained products YBO_3:Tb^{3+}, we find that the relative intensity of YBO_3:Tb^{3+} (Y:Tb = 8:2, 7:3, in molar ratio) is 600, 340 a.u., respectively, their values are higher than the commercial phosphor. It suggests that the products may have potential applications. The top right corner (Fig. 6) shows the scheme of energy transfer of Tb^{3+}. The luminescence provides us additional proof that the as-formed products are not mixture of $LnBO_3$ (Ln = Y, Tb), but that the Tb^{3+} ions have successfully entered the host crystal lattice as an activator under the hydrothermal process. Furthermore, it is interesting to discover that the emission spectra of the YBO_3:Tb^{3+} samples emit different light under VUV excitation with the different molar ratio of Y–Tb [Y:Tb = 8:2 (white); 7:3 (green); 6:4 (red); 5:5 (red); 4:6 (green)]. We found that when the Y/Tb value is 4, YBO_3:Tb^{3+} exhibits strong white emission under VUV light and the highest emission at 545 nm is corresponding to $^5D_4 \rightarrow {}^7F_5$ while for the Y/Tb value 1, YBO_3:Tb^{3+} exhibits strong red emission and the highest emission at 593 nm is corresponding to $^5D_4 \rightarrow {}^7F_4$. With decreasing the molar ratio of Y–Tb, YBO_3:Tb^{3+} samples show the different luminescent intensity of the $^5D_4 \rightarrow {}^7F_J$ transitions. As a result, the photoluminescence color can be tuned from white, red, to green by simply adjusting the molar ratio of Y–Tb.

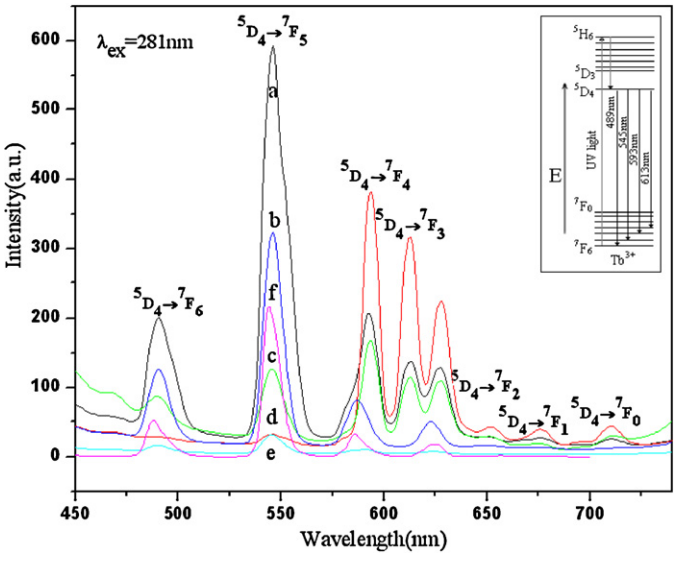

Fig. 6. Emission spectrum of YBO_3:Tb^{3+} samples with the different molar ratio of Y–Tb [Y:Tb = 8:2 (a); 7:3 (b); 6:4 (c); 5:5 (d); 4:6 (e)]; (f) emission spectra of the commercial phosphor $CeMgAl_{11}O_{19}$:Tb.The top right corner shows the scheme of energy transfer of Tb^{3+}.

4. Conclusions

In summary, a simple and mild hydrothermal method has been demonstrated for the synthesis of the fine, dispersed and homogeneous YBO_3:Tb^{3+} microflower structures assembled from YBO_3:Tb^{3+} nanoflakes. The reaction mechanism has been considered as a dissolution/precipitation mechanism; the self-assembly evolution process has been proposed on a homocentric layer-by-layer growth style. Due to the different luminescent intensity with the different molar ratio of Y–Tb, YBO_3:Tb^{3+} phosphors exhibit different light (white, red, green) under ultraviolet excitation, which might find potential applications in the fields such as light display systems and optoelectronic devices.

Acknowledgements

This work was supported by the Hubei Province Nature Science Foundation (2010CDB04701) and the Hubei Province Education Office Key Research (D20101011, D20091006) of China.

References

[1] H.L. Zhu, L. Zhang, T.T. Zuo, X.Y. Gu, Z.K. Wang, et al., Appl. Surf. Sci. 254 (2008) 6362–6365.
[2] F.S. Chen, C.H. Hsu, C.H. Lu, J. Alloys Compd. 505 (2010) L1–L5.
[3] Z. Yang, Y.L. Wen, N. Sun, Y.F. Wang, Y. Huang, Z.H. Gao, Y. Tao, J. Alloys Compd. 489 (2010) L9–L12.
[4] K. Suchinder, S. Sharma, M. Shreyas, M.S. Pitale, R.N. Manzar Malik, Qureshi, Dubey, J. Alloys Compd. 482 (2009) 468–475.
[5] G. Jia, H.P. You, K. Liu, Y.H. Zheng, N. Guo, J.J. Jia, H.J. Zhang, Chem. Eur. J. 16 (2010) 2930–2937.
[6] L. Chen, G.T. Yang, J.Q. Liu, X. Shu, G.B. Zhang, Y. Jiang, J. Appl. Phys. 105 (2009), 013513–013513-5.
[7] C. Mansuy, J.M. Nedelec, C. Dujardin, R. Mahiou, Opt. Mater. 29 (2007) 697–702.
[8] C. Jia, E. Xie, J. Zhao, Z. Sun, A. Peng, J. Appl. Phys. 100 (2) (2006), 023529-1–123529-5.
[9] K.Y. Jung, E.J. Kim, Y.C. Kang, J. Electrochem. Soc. 151 (3) (2004) H69–H73.
[10] L. Wang, L. Shi, N. Liao, H. Ji, P. Du, Z. Xi, L. Wang, D. Jin, Maters. Chem. Phys. 119 (2010) 490–494.

[11] J. Yang, C.M. Zhang, L.L. Wang, Z.Y. Hou, S.S. Huang, H.Z. Lian, J. Lin, J. Solid State Chem. 181 (2008) 2672–2680.
[12] Z.H. Li, J.H. Zeng, G.C. Zhang, Y.D. Li, J. Solid State Chem. 178 (2005) 3624–3630.
[13] J. Yang, C.X. Li, X.M. Zhang, Z.W. Quan, C.M. Zhang, H.Y. Li, J. Lin, Chem. Eur. J. 14 (2008) 4336–4345.
[14] W.B. Bu, Y.P. Xu, D.Y. Jiang, J.L. Shi, J. Phys. Chem. C 111 (2007) 5014–5019.
[15] L. Xu, C.L. Lu, Z.H. Zhang, X.Y. Yang, W.H. Hou, Nanoscale 2 (2010) 995–1005.
[16] Q.F. Lu, H.B. Zeng, Z. Wang, X.L. Cao, L.D. Zhang, Nanotechnology 17 (2006) 2098–2104.
[17] L.B. Feng, A.H. Liu, M. Liu, Y.Y. Ma, J. Wei, B.Y. Man, J. Alloys Compd. 492 (2010) 427–432.
[18] Z.H. Xu, C.X. Li, G.G. Li, R.T. Chai, C. Peng, D.M. Yang, J. Lin, J. Phys. Chem. C 114 (2010) 2573–2582.
[19] L. Ma, W.X. Chen, X.Y. Xu, L.M. Xu, X.M. Ning, Mater. Lett. 64 (2010) 1559–1561.
[20] S.Y. Hou, Y. Xing, H. Ding, X.C. Liu, B. Liu, X.J. Sun, Mater. Lett. 64 (2010) 1503–1505.
[21] E. Kowsari, G. Faraghi, Res. Bull. 45 (2010) 939–945.
[22] L.X. Yang, Y.J. Zhu, L. Li, L. Zhang, H. Tong, W.W. Wang, G.F. Cheng, J.F. Zhu, Eur. J. Inorg. Chem. 23 (2006) 4787–4792.
[23] J. Wang, Y.H. Xu, M. Hojamberdiev, M.Q. Wang, G.Q. Zhu, Maters. Chem. Phys. 119 (2010) 169–174.
[24] X. Guo, Y.H. Wang, J.C. Zhang, J. Cryst. Growth 311 (2009) 2409–2417.
[25] L.S. Zhong, J.S. Hu, H.P. Liang, A.M. Cao, W.G. Song, L.J. Wan, Adv. Mater. 18 (2006) 2426–2431.
[26] J. Yang, G.G. Li, C. Peng, C.X. Li, C.M. Zhang, Y. Fan, Z.H. Xu, Y. Cheng, J. Lin, J. Solid State Chem. 183 (2010) 451–457.
[27] H. Zhu, D. Yang, H. Yang, L. Zhu, D. Li, D. Jin, K. Yao, J. Nanopart. Res. 10 (2008) 307–312.